Chapter 3

The extended escape probability approach: the effect of a variable source function

Escape probability techniques for modelling and interpreting spectral emission from optically thick plasmas are potentially very useful. If they can be shown to be valid for a particular set of circumstances then the equations of radiative transfer and statistical balance are naturally linearised and decoupled. This comparative simplicity that escape probability methods introduce is desirable if they are to be used for studying such complex plasmas as those in the chromosphere and TR where there is much detailed structure and flow.

It is clear, however, that the expressions and methods presented thus far are insufficient to completely describe the SOHO-SUMER limb observations discussed in sec 2.3 and 2.4. When coupled with simple atmosphere models the line-of-sight averaged escape probability ($\bar{g}\{\tau_0\}$) is effective in modelling the opacity sensitive C II and C III branching ratios but is ineffective in regard to the observed fluxes. Departures of modelled from observed values occurred at and beyond the limb. These discrepancies must be due to the assumptions within the escape probability expressions and/or the atmosphere model. These assumptions relate to

1. variation of the source function

2. atmospheric structure

3. instrumental effects

In order to develop the escape probability methods it is important to consider each of the underlying assumptions to detect sources of error and to determine regimes of validity. Item 1 above incorporates variations of the source function with respect to both space and frequency due to absorption, scattering, line blending and flow. In this chapter, the variation of the source function with respect to space only is considered. In the subsequent chapters the frequency dependence of the source function will be addressed as well as items 2 and 3 above.

3.1 The source function

The source function, $S_\nu(\mathbf{x})$, is the ratio at $\mathbf{x}$ of the emissivity (emission coefficient) to the opacity (absorption coefficient) and is therefore given by

$$S_\nu(\mathbf{x}) = \frac{j_\nu(\mathbf{x})}{\kappa_\nu(\mathbf{x})} \tag{3.1}$$

$$= \frac{\omega_l}{\omega_u}\frac{2\nu^2}{c^2}\frac{\phi_e(\nu)}{\phi_a(\nu)}\frac{N_u(\mathbf{x})}{N_l(\mathbf{x})} \tag{3.2}$$

The variation of $S_\nu(\mathbf{x})$ in space follows that of $N_u(\mathbf{x})/N_l(\mathbf{x})$. In optically thin conditions this ratio is dependent on electron temperature and density but in thick conditions it is also influenced by opacity since photo-absorption will generally enhance N_u and deplete N_l.

Following the implications of fig. 2.15, the VAL atmosphere is not considered to be an appropriate model in regard to the C II and C III emission. However, envisaged here are C II and C III emission layers that comprise of TR sheaths around spicule-like structures and the VAL atmosphere model is adopted to represent each sheath. In optically thin conditions, the emission in a line versus temperature is described by the $G(T_e)$ function (see sec. 2.4.2). $G(T_e)$ functions versus T_e are shown in fig. 3.1 for the C II $2s^2 2p\,^2P_{3/2} - 2s2p^2\,^2P_{3/2}$ line at 904.143 Å and the C III $2s2p^3P_2$ - $2p^2\,^3P_2$ line at 1175.711 Å. The temperature range where these functions

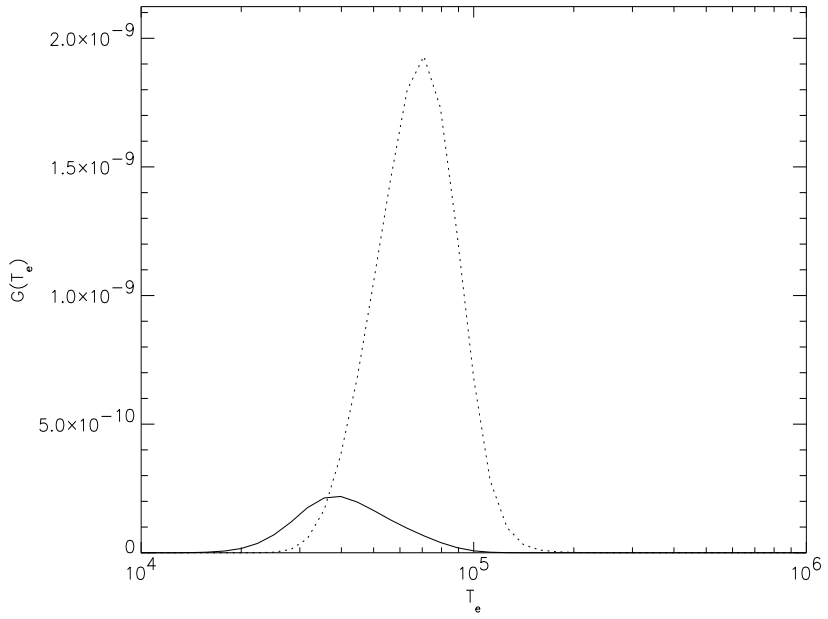

Figure 3.1: $G(T_e)$ functions for the C II $2s^2 2p^2 P_{3/2} - 2s2p^2\,^2P_{3/2}$ line at 904.143 Å (solid line) and the C III $2s2p^3 P_2$ - $2p^{2\,3}P_2$ line at 1175.711 Å (dotted line).

are non-negligible corresponds to a very narrow region in the VAL model and thus the sheaths predicted by this model are very thin. However, the electron density also varies rapidly over such regions and so even though the spatial extent of each sheath is small, the variation of electron density within them is significant. This is illustrated in figs 3.2a and b which show $G(T_e(N_e)) \times N_e$ versus N_e for both C II and C III. These functions are related to the *optically thin contribution functions* and are indicative of the degree of spectral emission as a function of electron density. It is evident from these that the electron density varies significantly over the region of line formation. Figs 3.3a and b show optically thin population density ratios versus electron density for C II $2s2p^{2\,2}P_{3/2}/2s^2 2p^2 P_{3/2}$ and C III $2p^{2\,3}P_2/2s2p^3 P_2$ with the $G(T_e(N_e)) \times N_e$ functions of figs 3.2a and b overlaid. From these it is clear that the ratios (and thus also the source function in each case) vary by several orders of magnitude over the region of line formation.

Consider a point in the emitting layer for either C II and C III and consider a

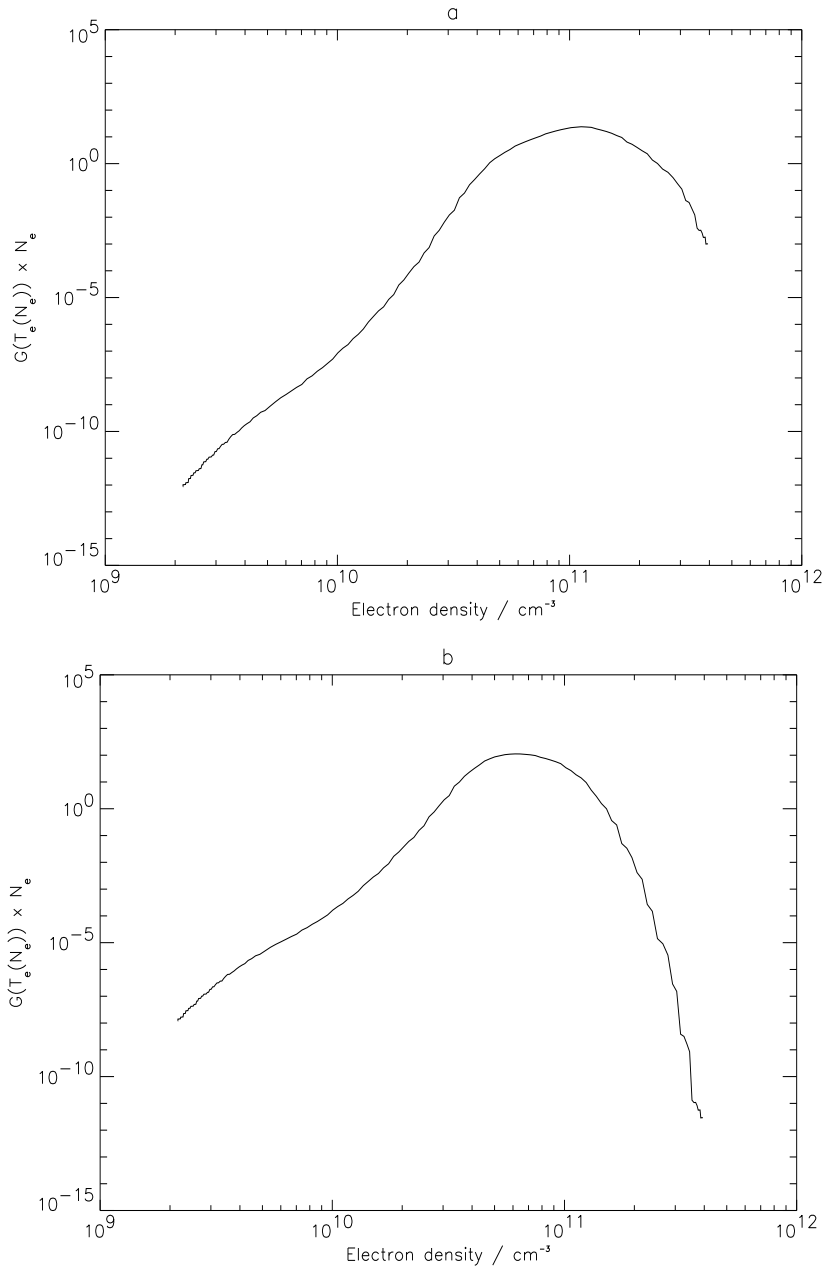

Figure 3.2: $G(T_e(N_e)) \times N_e$ versus N_e on a log-log scale for (a) the C II $2s^2 2p\,^2P_{3/2} - 2s2p^2\,^2P_{3/2}$ line at 904.143 Å and (b) the C III $2s2p^3P_2$ - $2p^{2\,3}P_2$ line at 1175.711 Å. $T_e(N_e)$ follows from the VAL atmosphere model. These functions are related to the optically thin contribution functions.

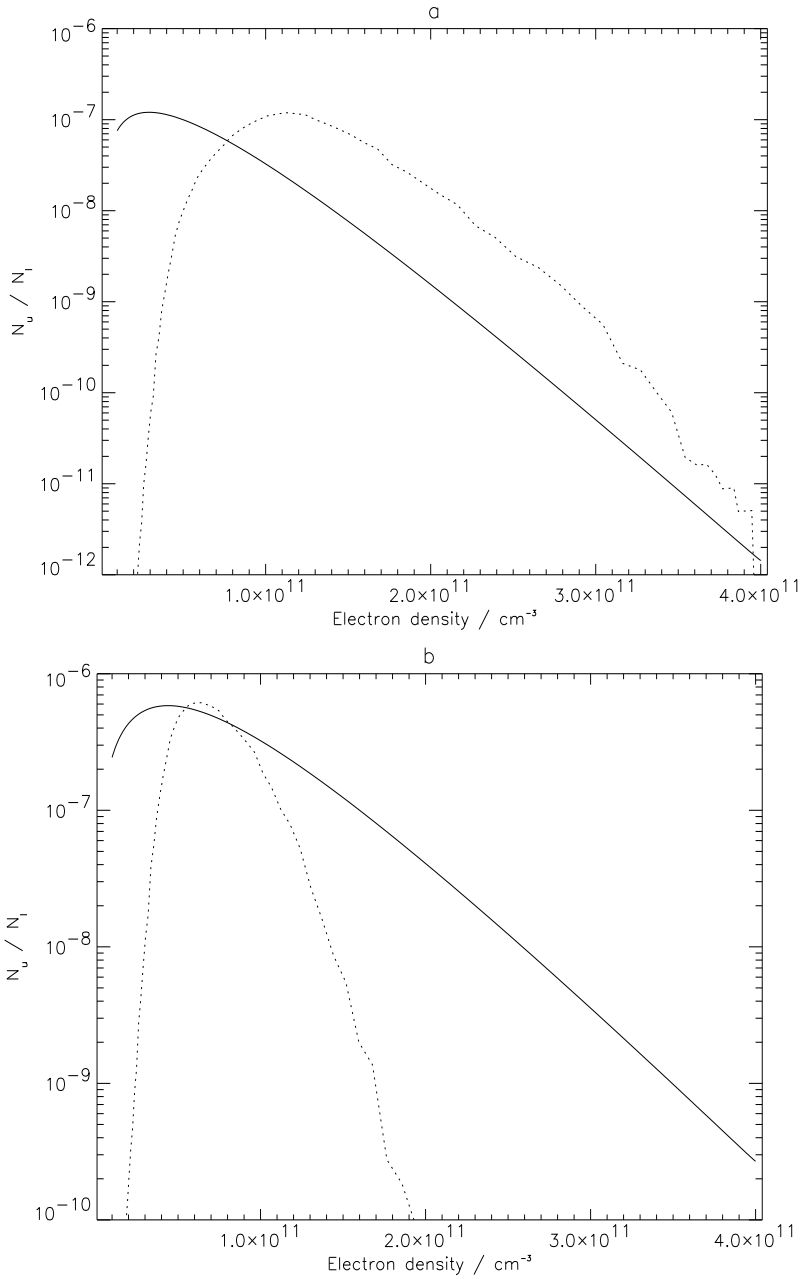

Figure 3.3: Optically thin population density ratios versus electron density on a log-log scale for (a) C II $2s2p^2\,^2P_{3/2}/2s^22p^2P_{3/2}$ and (b) C III $2p^2\,^3P_2/2s2p^3P_2$. These ratios are indicative of the dependence of the corresponding source functions upon electron density. The dotted lines correspond to $G(T_e(N_e)) \times N_e$ as in figs 3.2a and b, scaled to fit the plot in order to indicate the optically thin region of line formation. In both the C II and C III cases the population ratios vary several orders of magnitude over the region of line formation.

ray from that point leading out of the plasma. This ray will in general intersect many structures with sheaths as described. Consequently the source function will oscillate with respect to position along the ray. However, it will not, in optically thin circumstances, vary with position along the length of the spicule-like structures. Since the length of these structures is in general much larger than the thickness of the surrounding sheaths, the dependence of the source function on electron density is ignored here. Rather it is assumed that the population structure throughout the sheath is represented by one (T_e, N_e) pair, namely the temperature corresponding to the peak of the $G(T_e)$ function and the density at this temperature implied by the VAL model. This assumption seems severe but will be justified from observations in chapter 6.

Making this assumption enables the examination, within an escape probability picture, of the variation of the source function due to photo-absorption. In other words, this assumption allows focus to be made on the effect of scattering *into* the line-of-sight. For this eqs 2.7 and 2.8 must be revisited.

3.2 The spatially resolved absorption factor

3.2.1 $\bar{\bar{g}}\{\tau_0\}$ as a function of space

The picture considered here in regard to the effect of opacity upon the populations structure, is that of a semi-infinite plane-parallel slab. Within such a plasma the population structure will in general be dependent on height within the layer. The absorption factor expression developed in chapter 2, namely $\bar{\bar{g}}\{\tau_0\}$, predicts this even though this quantity itself was derived assuming that both the upper and lower level population densities are constant – i.e. that the population structure is independent of spatial position. By symmetry $\bar{\bar{g}}\{\tau_0\}$ may be written as a function of space. Consider absorption at the point x_0 in a slab of thickness D, due to the portion of the emitting layer defined by $0 \leq x \leq x_0$. The corresponding absorption factor is

$$\begin{aligned}\bar{\bar{g}}^{-}\{\tau_0^{-}(x_0)\} &= \frac{1}{2}\frac{1}{\sqrt{\pi}}\int_{-\infty}^{\infty} e^{-u^2}\Big[exp\left\{-\tau_0^{-}(x_0)e^{-u^2}\right\} - \\ &\quad \left\{\tau_0^{-}(x_0)e^{-u^2}\right\} E_1\left\{\tau_0^{-}(x_0)e^{-u^2}\right\}\Big]du \\ &= \frac{1}{2}\bar{\bar{g}}\{\tau_0^{-}(x_0)\} \end{aligned} \tag{3.3}$$

where

$$\tau_0^{-}(x_0) = \kappa_0 x_0 \tag{3.4}$$

A similar result follows for the portion of the emitting layer defined by $x_0 \leq x \leq D$ giving

$$\bar{\bar{g}}\{\tau_0/2\} = \frac{1}{2}\left(\bar{\bar{g}}\{\tau_0^{+}(x_0)\} + \bar{\bar{g}}\{\tau_0^{-}(x_0)\}\right) \tag{3.5}$$

where

$$\tau_0^{+}(x_0) = \kappa_0(D - x_0) \tag{3.6}$$

It follows therefore that a spatially dependent absorption factor, $\mathcal{G}(\tau_0, x)$, may be defined as

$$\mathcal{G}(\tau_0, x) = \frac{1}{2}\left(\bar{\bar{g}}\{\tau_0^{+}(x)\} + \bar{\bar{g}}\{\tau_0^{-}(x)\}\right) \tag{3.7}$$

Fig. 3.4 shows $\mathcal{G}(\tau_0, x)$ versus τ_0 for $x = 0$ and $x = D/2$ from which it is clear that $\mathcal{G}(\tau_0, x)$ is indeed spatially dependent. This illustrates that for $\tau_0 \neq 0$ the population structure differs at layer edge compared to layer centre and thus the ratio of upper to lower level population density varies throughout the layer. This in turn violates the constant density assumption that underpins the $\mathcal{G}(\tau_0, x)$ expression.

3.2.2 Inclusion of variable density in the absorption factor expression

For $\mathcal{G}(\tau_0, x)$ to be valid both the upper and lower level population densities must be constant. If this assumption is not made then the *spatially resolved* absorption factor is obtained.

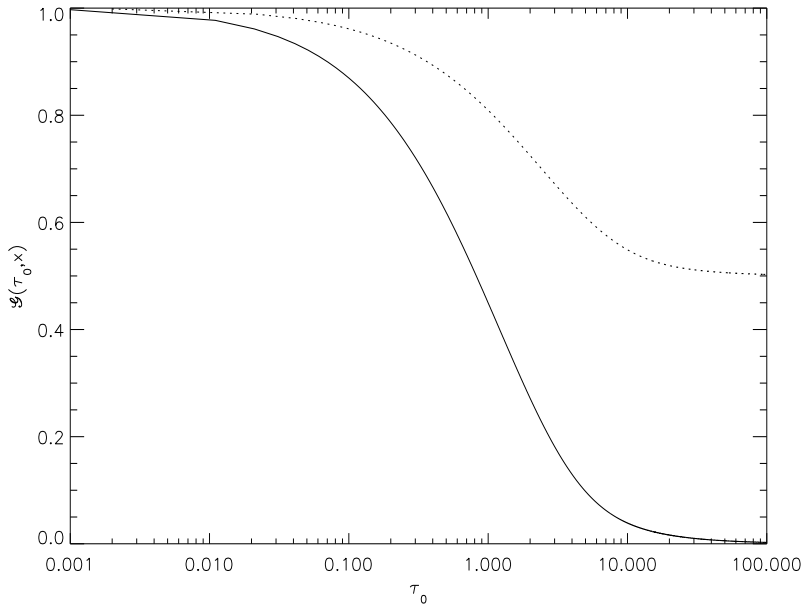

Figure 3.4: $\mathcal{G}(\tau_0, x)$ versus τ_0 for $x = 0$ (solid line) and $x = D/2$ (dotted line).

For a stratified atmosphere it may be written that $N_l \equiv N_l(x)$. The probability, dT_ν, that a photon of frequency ν emitted at point x in the layer will propagate a distance dl at an angle θ to the x-axis is

$$dT_\nu(x, \theta, dl) = exp(-\kappa_\nu(x) dl) \tag{3.8}$$

$$= exp(-\kappa_\nu(x) dx/cos\theta) \tag{3.9}$$

The probability that the photon will propagate a further distance dl is

$$dT_\nu(x, \theta, 2dx/cos\theta) = exp(-\kappa_\nu(x) dx/cos\theta) \times exp(-\kappa_\nu(x + dx) dx/cos\theta) \tag{3.10}$$

$$= exp(-[\kappa_\nu(x) + \kappa_\nu(x + dx)] dx/cos\theta) \tag{3.11}$$

Following this, the probability, T_ν, that a photon of frequency ν emitted at the point x in the layer will propagate a distance l at an angle θ to the x-axis is

$$T_\nu(x, \theta, l) = exp\left(-\frac{1}{cos\theta} \int_x^{x_1} \kappa_\nu(x') dx'\right) \tag{3.12}$$

where $x_1 = x + lcos\theta$.

The intensity, dI_ν at $\mathbf{x} = (x_0, 0)$ due to the volume element dV is

$$\begin{aligned}
dI_\nu(\mathbf{x}) &= \frac{j_\nu(\mathbf{r})}{|\mathbf{r}-\mathbf{x}|^2} exp\left\{-\int_{\mathbf{r}\to\mathbf{x}} \kappa_\nu(\mathbf{r})dl\right\} dV \\
\Rightarrow I_\nu(\mathbf{x_0}) &= \frac{1}{4\pi}\int\int_V\int \frac{j_\nu(x)}{l^2} exp\left\{-\frac{l}{x}\int_x^{x_0}\kappa_\nu(x')dx'\right\} dV \\
&= \frac{1}{4\pi}\int_0^{2\pi}\left[\int_0^{x_0}\int_x^\infty \frac{j_\nu(x)}{l^2} exp\left\{-\frac{l}{x}\int_x^{x_0}\kappa_\nu(x')dx'\right\} ldldx\right. \\
&\quad \left. + \int_{x_0}^{D}\int_x^\infty \frac{j_\nu(x)}{l^2} exp\left\{-\frac{l}{x}\int_{x_0}^{x}\kappa_\nu(x')dx'\right\} ldldx\right] d\theta \\
&= \frac{1}{2}\left[\int_0^{x_0} j_\nu(x) E_1\left\{\int_x^{x_0}\kappa_\nu(x')dx'\right\} dx\right. \\
&\quad \left. + \int_{x_0}^{D} j_\nu(x) E_1\left\{\int_{x_0}^{x}\kappa_\nu(x')dx'\right\} dx\right] \qquad (3.13)
\end{aligned}$$

Thus, from eq. 2.6,

$$\begin{aligned}
\Lambda(\tau_0, x_0) = 1 &- \frac{1}{2}\frac{N_l(x_0)}{N_u(x_0)}\frac{\omega_u}{\omega_l}\frac{c^2}{2\nu_0^2}\int\phi(\nu)\left[\int_0^{x_0} j_\nu(x)E_1\left\{\int_x^{x_0}\kappa_\nu(x')dx'\right\}dx\right. \\
&+ \left.\int_{x_0}^{D} j_\nu(x)E_1\left\{\int_{x_0}^{x}\kappa_\nu(x')dx'\right\}dx\right]d\nu \qquad (3.14)
\end{aligned}$$

Using the relation between $j_\nu(x)$ and $\kappa_\nu(x)$ specified in eq. 2.32, and considering purely Doppler broadened profiles, this becomes

$$\begin{aligned}
\Lambda(\tau_0, x_0) = 1 &- \frac{1}{2\sqrt{\pi}}\frac{N_l(x_0)}{N_u(x_0)}\int e^{-2u^2}\left[\int_0^{x_0} N_u(x)\kappa_0 E_1\left\{e^{u^2}\tau_0(x, x_0)\right\}dx\right. \\
&+ \left.\int_{x_0}^{D} N_u(x)\kappa_0 E_1\left\{e^{u^2}\tau_0(x_0, x)\right\}dx\right]d\nu \qquad (3.15)
\end{aligned}$$

Eq. 3.15 is the absorption factor at the point x_0 in a semi-infinite plane-parallel slab. No assumption is made here about the density, nor the variation of the source function with respect to space. This expression reintroduces nonlinearity and coupling to the radiative transfer equations. Therefore it must be solved iteratively.

The absorption factor has a functional dependence on the optical depth quantities $\tau_0(x_1, x_2)$ defined as

$$\tau_0(x_1, x_2) = \kappa_0\int_{x_1}^{x_2} N_l(x)dx \qquad (3.16)$$

However, for a particular lower level population density distribution, the absorption factor at the point x_0 is prescribed by the total optical depth, $\tau_0 \equiv \tau_0(0, D)$, and so is denoted $\Lambda(\tau_0, x_0)$.

3.2.3 Verification of the Λ result

Eq. 3.15 may be checked by considering the case where both N_u and N_l are constant in space. In this case, $\Lambda(\tau_0, D/2) \equiv \bar{\bar{g}}\{\tau_0/2\}$, viz.

$$\begin{aligned}
\Lambda(\tau_0, D/2) &= 1 - \frac{2}{2\sqrt{\pi}} \frac{N_l}{N_u} N_u \kappa_0 \int_{-\infty}^{\infty} e^{-2u^2} \int_0^{D/2} E_1 \left\{ \kappa_0 N_l (D/2 - x) e^{-u^2} \right\} dx du \\
&= 1 - \frac{N_l \kappa_0}{\sqrt{\pi}} \int_{-\infty}^{\infty} e^{-2u^2} \int_0^{D/2} \int_x^{\infty} \frac{e^{l \kappa_0 N_l e^{-u^2}}}{l} dl dx du \\
&= 1 - \frac{N_l \kappa_0}{\sqrt{\pi}} \int_{-\infty}^{\infty} e^{-2u^2} \left[\int_0^{D/2} \int_0^{l} \frac{e^{l \kappa_0 N_l e^{-u^2}}}{l} dx dl + \int_{D/2}^{\infty} \int_0^{D/2} \frac{e^{l \kappa_0 N_l e^{-u^2}}}{l} dx dl \right] du \\
&= 1 - \frac{N_l \kappa_0}{\sqrt{\pi}} \int_{-\infty}^{\infty} e^{-2u^2} \left[\int_0^{D/2} e^{l \kappa_0 N_l e^{-u^2}} dl + \int_{D/2}^{\infty} \frac{D}{2} \frac{e^{l \kappa_0 N_l e^{-u^2}}}{l} dl \right] du \\
&= 1 - \frac{N_l \kappa_0}{\sqrt{\pi}} \int_{-\infty}^{\infty} e^{-2u^2} \left[-\frac{e^{D \kappa_0 N_l e^{-u^2}/2}}{\kappa_0 N_l e^{-u^2}} + \frac{1}{\kappa_0 N_l e^{-u^2}} + \frac{D}{2} E_1 \left\{ \kappa_0 N_l e^{-u^2} \right\} \right] du \\
&= \frac{1}{\sqrt{\pi}} \int_{-\infty}^{\infty} e^{-u^2} \left[exp \left\{ -\frac{\tau_0}{2} e_{-u^2} \right\} - \frac{\tau_0}{2} e^{-u^2} E_1 \left\{ \frac{\tau_0}{2} e^{-u^2} \right\} \right] du \\
&\equiv \bar{\bar{g}}\{\tau_0/2\}
\end{aligned} \tag{3.17}$$

3.3 The assumption of constant source function

The results discussed above provide a route to obtaining an optically thick upper level population distribution via calculation of the spatially resolved absorption factor, $\Lambda(\tau_0, x_0)$ (eq. 3.15). Using this upper level population distribution, optically thick emergent fluxes may then be calculated via

$$I = \frac{1}{4\pi} A_{u \to l} \int_{l.o.s} N_u(s) g\{\tau_0(s)\} ds \tag{3.18}$$

Thus it is possibly to assess directly the implications of assuming that the source function is constant in space.

The impact of this assumption is profound. If it is made, then eqs 2.17 and 2.38 (i.e. $\bar{g}\{\tau_0\}$ and $\bar{\bar{g}}\{\tau_0/2\}$) may be extended into the variable density case as follows: consider emission along a line-of-sight of length L. If an element of distance along this line-of-sight is denoted ds then eq. 3.18 may be written as

$$I \sim \int_0^L N_u(s) g\{\tau_0(s)\} ds \tag{3.19}$$

with

$$\tau_0(s) = \kappa_0 \int_0^s N_l(s') ds' \tag{3.20}$$

Since it is assumed that the source function is constant, it may be written that

$$\frac{N_u(s)}{N_l(s)} = R = const \tag{3.21}$$

If $\bar{N}_u$ and $\bar{N}_l$ are defined as

$$\begin{aligned} \bar{N}_u &= \frac{\int_0^L N_u(s) ds}{L} \\ \bar{N}_l &= \frac{\int_0^L N_l(s) ds}{L} \end{aligned} \tag{3.22}$$

then it follows that

$$\Rightarrow \frac{\bar{N}_u}{\bar{N}_l} = \frac{N_u(s)}{N_l(s)} = R \tag{3.23}$$

It is useful to define $\eta(s)$ as follows:

$$\begin{aligned} \eta(s) &= \frac{\int_0^s N_l(s') ds'}{\bar{N}_l} \\ \Rightarrow \frac{d\eta}{ds} &= \frac{N_l(s)}{\bar{N}_l} \\ \Rightarrow N_u(s) ds &= \bar{N}_u \frac{N_l(s)}{\bar{N}_l} ds = \bar{N}_u \frac{d\eta}{ds} ds \end{aligned} \tag{3.24}$$

Therefore

$$\begin{aligned} I &\sim \int_0^L \bar{N}_u g\{\kappa_0 \bar{N}_l \eta\} d\eta \\ &\sim \bar{N}_u \bar{g}\{\tau_0\} \end{aligned} \tag{3.25}$$

It may also be shown that $\bar{g}\{\tau_0\}$ is valid if the source function is constant with respect to space. As before

$$dI_\nu = \frac{j_\nu(\mathbf{x})}{l^2} exp\left\{-\int_{\mathbf{x}\rightarrow\mathbf{0}} \kappa_\nu(\mathbf{x}')d\mathbf{x}'\right\} dV \tag{3.26}$$

and

$$\bar{I}_\nu = \frac{1}{4\pi}\int\int_V\int dI_\nu \tag{3.27}$$

Consider the intensity, $\bar{I}_\nu^-$, due to the portion of the emitting layer defined by $0 \leq x \leq x_0$. This is given by

$$\bar{I}_\nu^- = \frac{1}{4\pi}\int_0^\pi\int_0^{x_0}\int_{x_0}^\infty \frac{j_\nu(\mathbf{x})}{l^2} exp\left\{-\int_0^{x_0}\kappa_\nu(\mathbf{x}')d\mathbf{x}'\frac{l}{x}\right\} l dl dx d\theta \tag{3.28}$$

It is convenient to re-write this in spherical polar coordinates:

$$\begin{aligned}
\bar{I}_\nu^- &= \frac{1}{4\pi}\int_0^\pi 2\int_0^{\pi/2}\int_0^{x_0/cos\theta} \frac{j_\nu(r\,cos\theta)}{r^2} exp\left\{-\frac{1}{cos\theta}\int_0^{r\,cos\theta}\kappa_\nu(x)dx\right\} r^2 sin\theta dr d\theta d\phi \\
&= \frac{1}{2}\int_0^{\pi/2}\int_0^{x_0/cos\theta} \sigma\kappa_0 e^{-u^2}\frac{\bar{N}_u}{\bar{N}_l}N_l(r\,cos\theta) exp\left\{-\frac{1}{cos\theta}\int_0^{r\,cos\theta}\kappa_\nu(x)dx\right\} sin\theta dr d\theta
\end{aligned} \tag{3.29}$$

where

$$\sigma = \frac{\omega_l}{\omega_u}\frac{2\nu_0^2}{c^2} \tag{3.30}$$

Defining s as

$$s(r\,cos\theta) = \frac{\int_0^{x_0} N_l(x)dx}{x_0} \tag{3.31}$$

it then follows that

$$\begin{aligned}
\bar{I}_\nu^- &= \frac{1}{2}\int_0^{\pi/2}\int_0^{x_0}\sigma\kappa_0 e^{-u^2}\bar{N}_u exp\left\{-\frac{\kappa_0\bar{N}_l e^{-u^2}}{cos\theta}s\right\}\frac{sin\theta}{cos\theta}ds d\theta \\
&= \frac{1}{2}\frac{\bar{N}_u}{\bar{N}_l}\sigma\int_0^{\pi/2} sin\theta\left[1 - exp\left\{-\frac{\kappa_0\bar{N}_l x_0 e^{-u^2}}{cos\theta}\right\}\right] d\theta \\
&= \frac{1}{2}\frac{\bar{N}_u}{\bar{N}_l}\sigma\left[-cos\theta\Big|_0^{\pi/2} - \int_0^{\pi/2} sin\theta\, exp\left\{-\frac{\kappa_0\bar{N}_l x_0 e^{-u^2}}{cos\theta}\right\}\right] d\theta
\end{aligned}$$

$$
\begin{aligned}
&= \frac{1}{2}\frac{\bar{N}_u}{\bar{N}_l}\sigma\left[1-\int_1^\infty \frac{1}{t^2} exp\left\{-\kappa_0 \bar{N}_l x_0 e^{-u^2} t\right\} dt\right] \\
&= \frac{1}{2}\frac{\bar{N}_u}{\bar{N}_l}\sigma\left[1-E_2\kappa_0 \bar{N}_l x_0 e^{-u^2}\right] \\
&= \frac{1}{2}\frac{\bar{N}_u}{\bar{N}_l}\sigma\left[1+\frac{exp\left\{\kappa_0 \bar{N}_l x_0 e^{-u^2} t\right\}}{t}\Big|_1^\infty + \kappa_0 \bar{N}_l x_0 e^{-u^2}\int_1^\infty \frac{1}{t} exp\left\{\kappa_0 \bar{N}_l x_0 e^{-u^2} t\right\} dt\right] \\
&= \frac{1}{2}\frac{\bar{N}_u}{\bar{N}_l}\sigma\left[1-exp\{-\tau_0^- e^{-u^2}\}+\tau_0^- e^{-u^2} E_1\{\tau_0^- e^{-u^2}\}\right] \qquad (3.32)
\end{aligned}
$$

where

$$\tau_0^- = \kappa_0 \int_0^{x_0} N_l(x)dx$$
$$\tau_0^+ = \kappa_0 \int_{x_0}^{D} N_l(x)dx$$

Therefore,

$$\bar{\bar{g}}^-\{\tau_0^-\} = \frac{1}{2}-\frac{1}{2\sqrt{\pi}}\int_{-\infty}^{\infty} e^{-u^2}\left[exp\{-\tau_0^- e^{-u^2}\}-\tau_0^- e^{-u^2} E_1\{\tau_0^- e^{-u^2}\}\right] \qquad (3.33)$$

An analogous result exists for $\bar{\bar{g}}^+\{\tau_0^-\}$ and thus

$$\Lambda(\tau_0, x_0) = \left(\bar{\bar{g}}\{\tau_0^-\}+\bar{\bar{g}}\{\tau_0^+\}\right)/2 \equiv \mathcal{G}(\tau_0, x_0) \qquad (3.34)$$

3.4 The spatially resolved population calculation

Shown in figs 3.5 and 3.6 are absorption factors versus position for a selection of spectral lines of C II corresponding to three sets of optical depths. Since the absorption factors depend upon the optical depth rather than the geometrical thickness of the model plasma, and since plots are shown for three sets of optical depths, the x-axis is labelled *position index*. This relates to the computational grid and is equivalent to the geometric position in arbitrary units. The first step in their calculation is choosing a lower level population density distribution. This distribution describes the spatial variation of the lower level population densities of the optically thick lines. As discussed earlier, only lines whose lower levels are metastable are considered to be potentially thick and these levels are negligibly affected by opacity for the moderate optical depths considered here. Consequently the lower level population density

distributions remain constant throughout the calculation. From these, the optical depths, $\tau_0(x_1, x_2)$ may be calculated for each (x_1, x_2) pair, and these also remain constant throughout the calculation. An initial guess for $N_u(x)$ is then required. This is taken to be either the optically thin value – simply a multiple of $N_l(x)$ for each line – or the output of a previous iteration. However, any initial guess is valid (in principle) providing that convergence is subsequently achieved from it. From these $\Lambda(\tau_0, x)$ may be calculated for every line at each x via eq. 3.15. Then at each point the Λ's may be used to modify the Einstein A-coefficients in the statistical balance equations to obtain the optically thick population structure at each point in the layer. From this the optically thick upper level population distributions may be assembled via the lower level distributions which, as stated above, are unchanged.

3.5 The effect of an opacity modified source function upon the absorption factor

Inspection of eq. 3.15 reveals that it is not so much the value of the source function at a particular point that is important but rather the variation of the source function throughout the emitting layer. This can be seen by consideration of the $N_l(x_0)N_u(x)/N_u(x_0)$ term. It is not the value of $N_u(x)$ that matters, nor the ratio $N_u(x)/N_l(x)$ but rather the ratio $N_u(x)/N_u(x_0)$. The calculation is sensitive to this ratio – a fact that impinges upon its convergence (or otherwise).

Presented below is a brief summary of the characteristics of the absorption factors of lines of each of the C II multiplets containing optically thick lines.

The 1335 Å multiplet

The absorption factors of all three of these lines follow the $\mathcal{G}(\tau_0, x)$ trend broadly speaking. The most notable deviation is in the $2s^2 2p\,^2P_{3/2} - 2s2p^2\,^2D_{3/2}$ line at 1335.665 Å. This line shares its upper level with the $2s^2 2p\,^2P_{1/2} - 2s2p^2\,^2D_{3/2}$ line at 1334.524 Å but is less optically thick.

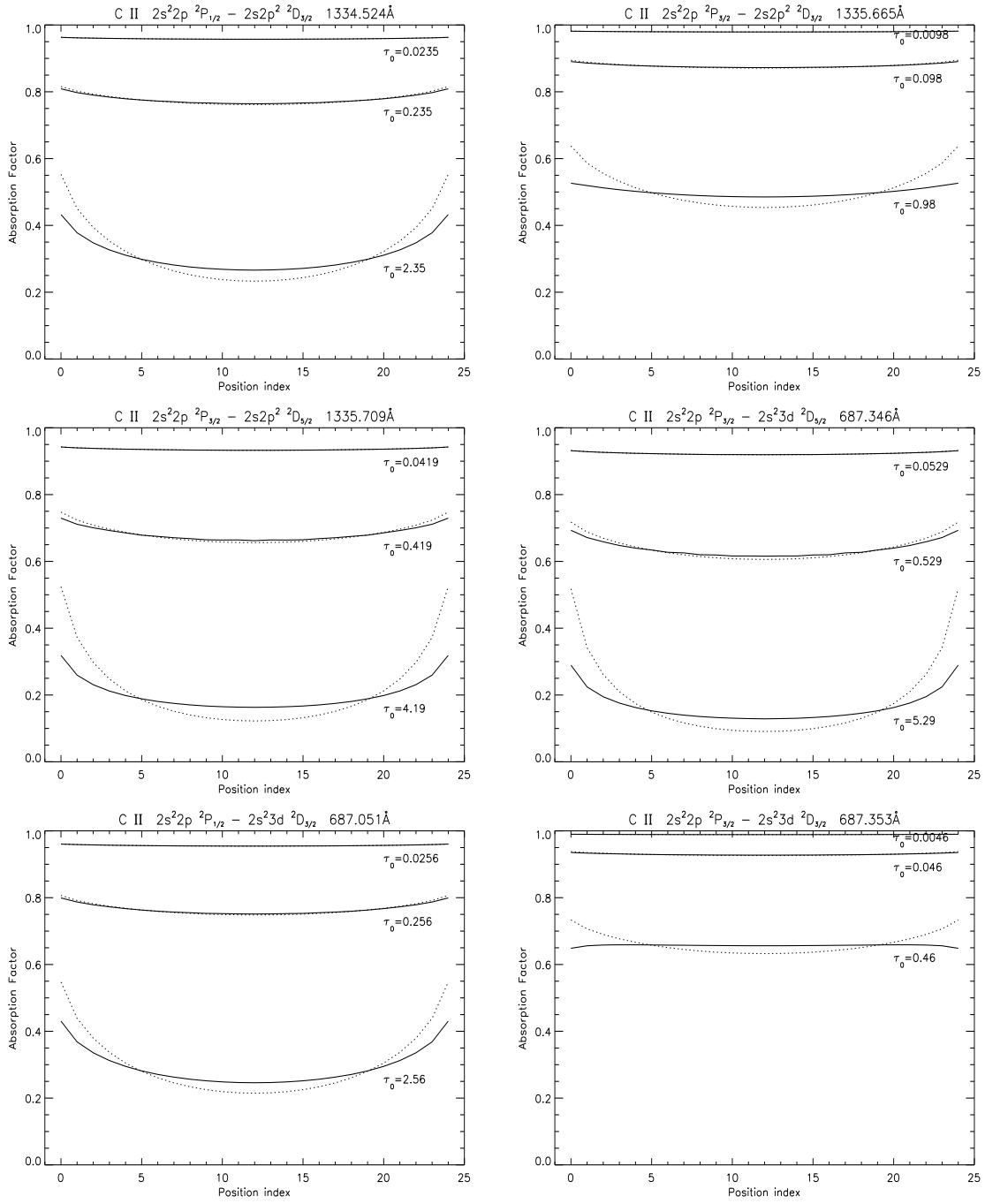

Figure 3.5: Absorption factors versus position for selected lines of C II corresponding to three sets of optical depths. Absorption factors are calculated iteratively via eqs 3.15 and 2.8. The solid lines are $\Lambda(\tau_0, x)$ and the dotted lines are $\mathcal{G}\{\tau_0, x\}$.

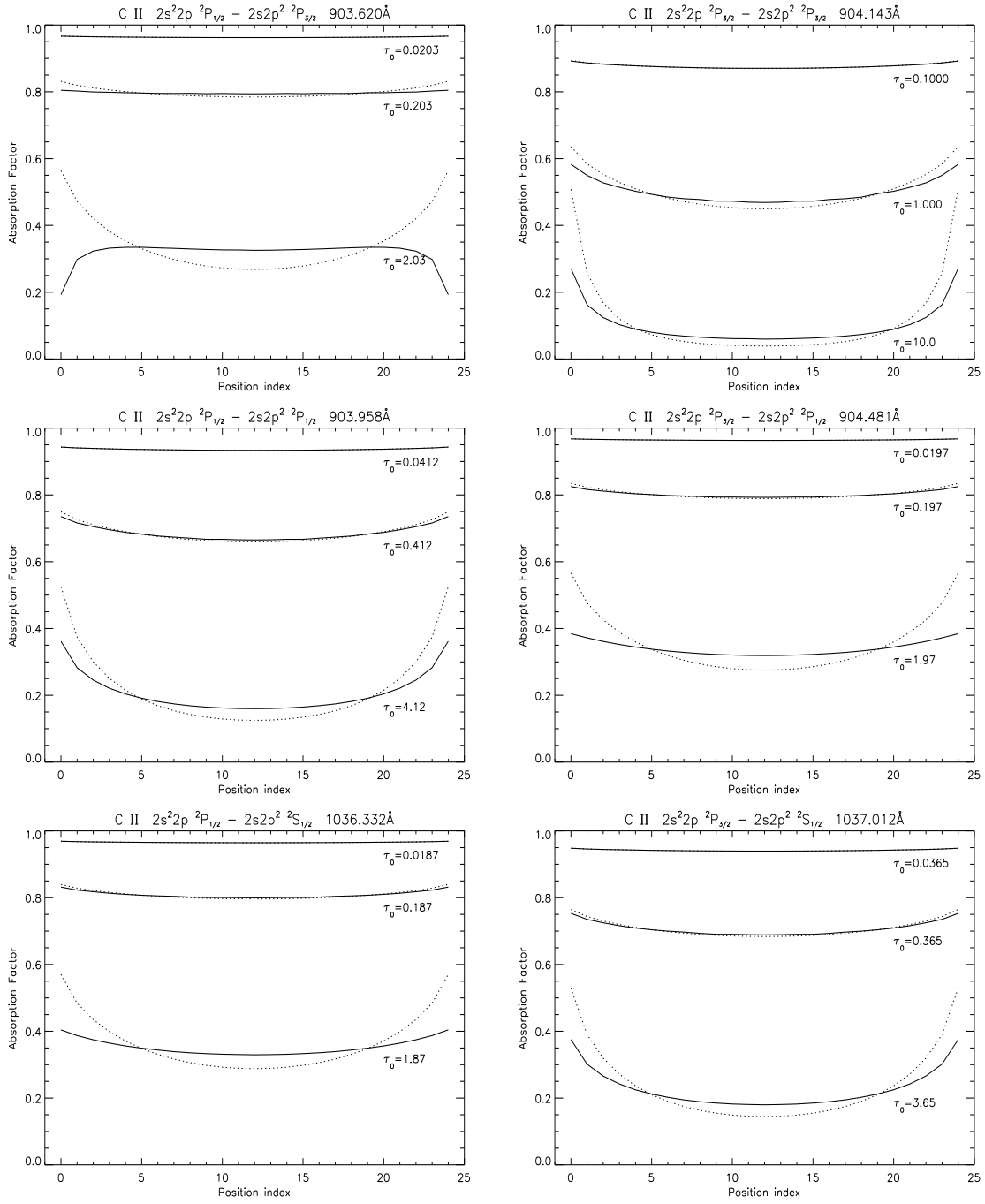

Figure 3.6: Absorption factors versus position for selected lines of C II as in fig 3.5.

The 687 Å multiplet

In this case the absorption factors of both the $2s^2 2p\,^2P_{3/2} - 2s^2 3d\,^2D_{5/2}$ line at 687.346 Å and the $2s^2 2p\,^2P_{1/2} - 2s^2 3d\,^2D_{3/2}$ line at 687.051 Å follow the $\mathcal{G}(\tau_0, x)$ trend. At an optical depth of 10 in the *control line* (the $2s^2 2p\,^2P_{3/2} - 2s 2p^2\,^2P_{3/2}$ line at 904.143 Å) the $2s^2 2p\,^2P_{3/2} - 2s^2 3d\,^2D_{3/2}$ line at 687.353 Å deviates from the $\mathcal{G}(\tau_0, x)$ trend. Again, this line shares its upper level with another (the 687.346 Å line) which is more optically thick.

The 904 Å multiplet

In this multiplet the absorption factors of two of the lines follow the $\mathcal{G}(\tau_0, x)$ trend and two deviate. The $2s^2 2p\,^2P_{3/2} - 2s 2p^2\,^2P_{3/2}$ line at 904.143 Å and the $2s^2 2p\,^2P_{3/2} - 2s 2p^2\,^2P_{1/2}$ line at 903.958 Å are the followers and they are also the most optically thick of the four lines. The $2s^2 2p\,^2P_{1/2} - 2s 2p^2\,^2P_{3/2}$ line at 903.620 Å and the $2s^2 2p\,^2P_{3/2} - 2s 2p^2\,^2P_{1/2}$ line at 904.481 Å are thinner and share upper levels with the 904.143 Å and 903.958 Å lines respectively.

The 1036 Å multiplet

Both the lines of the 1036 Å multiplet share an upper level and both follow the $\mathcal{G}(\tau_0, x)$ trend broadly speaking, one slightly more than the other. The one that deviates most markedly, namely the $2s^2 2p\,^2P_{1/2} - 2s 2p^2\,^2S_{1/2}$ line at 1036.332 Å, is, once again, the thinner of the two.

Discussion

In all the C II multiplets listed above there is a deviation in $\Lambda(\tau_0, x)$ from $\mathcal{G}(\tau_0, x)$ and in each this deviation is due to the distortion of $N_u(x)$ with respect to space (see figs 3.8 $\rightarrow$ 3.11). $\Lambda(\tau_0, x_0)$ depends on the integral of $N_u(x)/N_u(x_0)$ over x. Consequently $\Lambda(\tau_0, x_0) > \mathcal{G}(\tau_0, x_0)$ at layer centre since the population is most enhanced at this point – i.e. $N_u(x)/N_u(D/2) < 1$ for all $x \neq D/2$. Conversely, $\Lambda(\tau_0, x_0) < \mathcal{G}(\tau_0, x_0)$ at the edges since the population is least enhanced at these points – i.e. $N_u(x)/N_u(0) > 1$ and $N_u(x)/N_u(D) > 1$ for all $x \neq 0, D$. Thus there

is always a difference between the $\Lambda(\tau_0, x)$ and $\mathcal{G}(\tau_0, x)$ results since there is always at least *some* distortion of the upper level population distribution. Furthermore, this difference increases with optical depth since the distortion also increases with optical depth.

In each multiplet there are examples where the deviation of $\Lambda(\tau_0, x)$ from $\mathcal{G}(\tau_0, x)$ is particularly marked, in some instances reversing the $\mathcal{G}(\tau_0, x)$ versus x trend (e.g. the 903.620 Å line in fig. 3.6). In each of these cases the line in question shares its upper level with another, more optically thick line in the multiplet. In such circumstances both lines contribute to the deviation in the upper level density distribution due to reabsorption but more so the thicker line. Thus the upper level distribution is more significantly enhanced than it would be if just one of the lines were thick. It follows that for each line the population distribution is more distorted than it would be if that line were the only thick one and so the $\Lambda(\tau_0, x)$'s move further away from the corresponding $\mathcal{G}(\tau_0, x)$'s. This is true for all the lines stemming from the upper level in question but the effect is observed mostly in the thinner lines. This is because it is the thicker lines that make the most significant contribution to the upper level distortion and so the distortion itself is more consistent with the opacity in the thicker line than in the thinner ones.

3.6 The validity of $\mathcal{G}(\tau_0, x)$

The validity of $\mathcal{G}(\tau_0, x)$ can be found directly by looking for the region where the $\Lambda(\tau_0, x)$ results agree. This validity is evidently not a simple function of optical depth unless the line in question makes the dominant contribution to the upper level population enhancement with respect to all the other lines stemming from that same upper level.

Fig. 3.7 shows plots of $\Lambda(\tau_0, x)$ versus optical depth at layer centre and layer edge compared with $\mathcal{G}(\tau_0, x)$. For the C II spectral line classification (see table 2.6) the greatest optical depth was 1.76 for the $2s^2 2p\ ^2P_{3/2} - 2s2p^2\ ^2P_{3/2}$ line at 904.143 Å. This is in the regime where the deviation of $\Lambda(\tau_0, D/2)$ from $\mathcal{G}(\tau_0, D/2)$ ($\equiv \bar{\bar{g}}\{\tau_0/2\}$) is minimal. At layer centre $\Lambda(\tau_0, D/2)$ is close to being monotonic and is close to

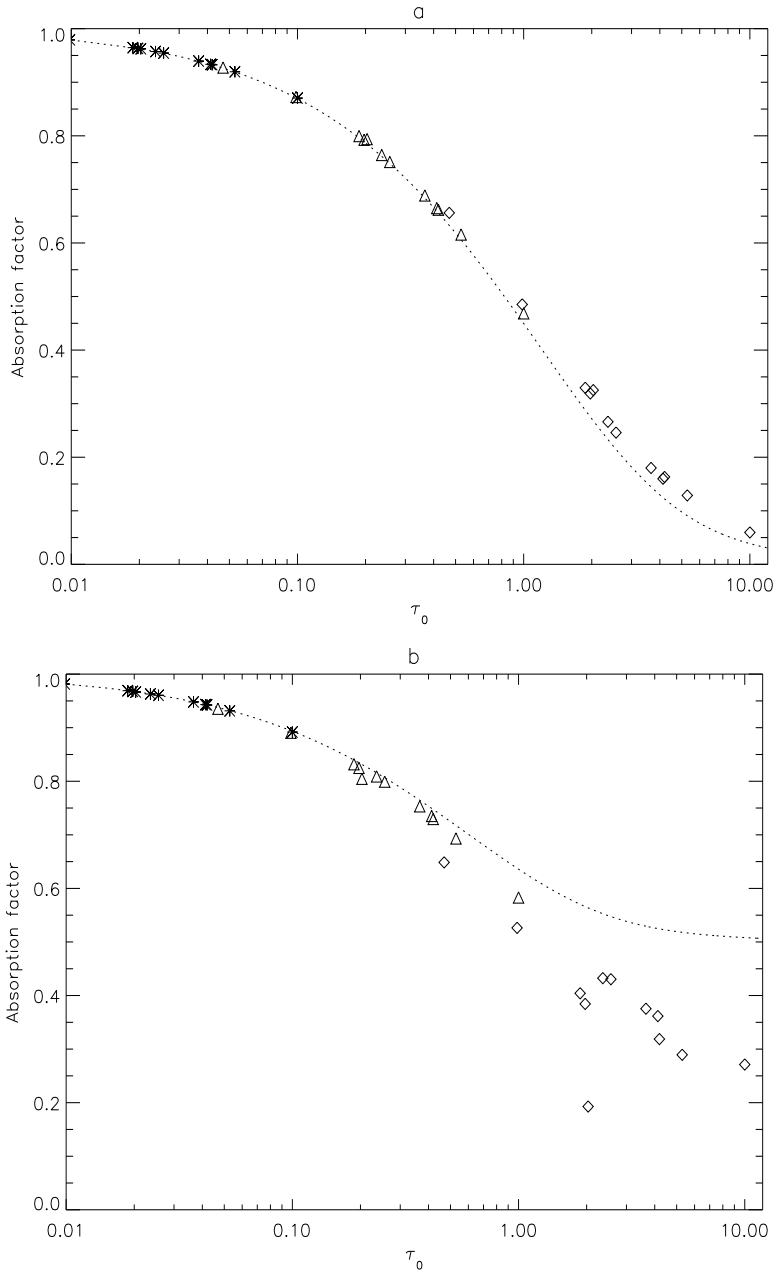

Figure 3.7: Absorption factors at (a) layer centre ($x = D/2$) and (b) layer edge ($x = 0$) versus optical depth for the constant lower level density model, taken from the plots in figs 3.5 and 3.6. The *'s, $\triangle$'s and $\diamond$'s are the absorption factors, $\Lambda(\tau_0, x)$, corresponding to the same three sets of optical depths as in figs 3.5 and 3.6. The dotted lines correspond to $\mathcal{G}(\tau_0, x)$.

$\mathcal{G}(\tau_0, D/2)$. At the edge, however, the variation of the source function becomes significant and $\mathcal{G}(\tau_0, 0)$ merely provides an upper limit to $\Lambda(\tau_0, 0)$. This figure shows $\mathcal{G}(\tau_0, x)$ to be a good approximation to $\Lambda(\tau_0, x)$ up to optical depths of around 0.5.

3.7 The effect upon the density distributions

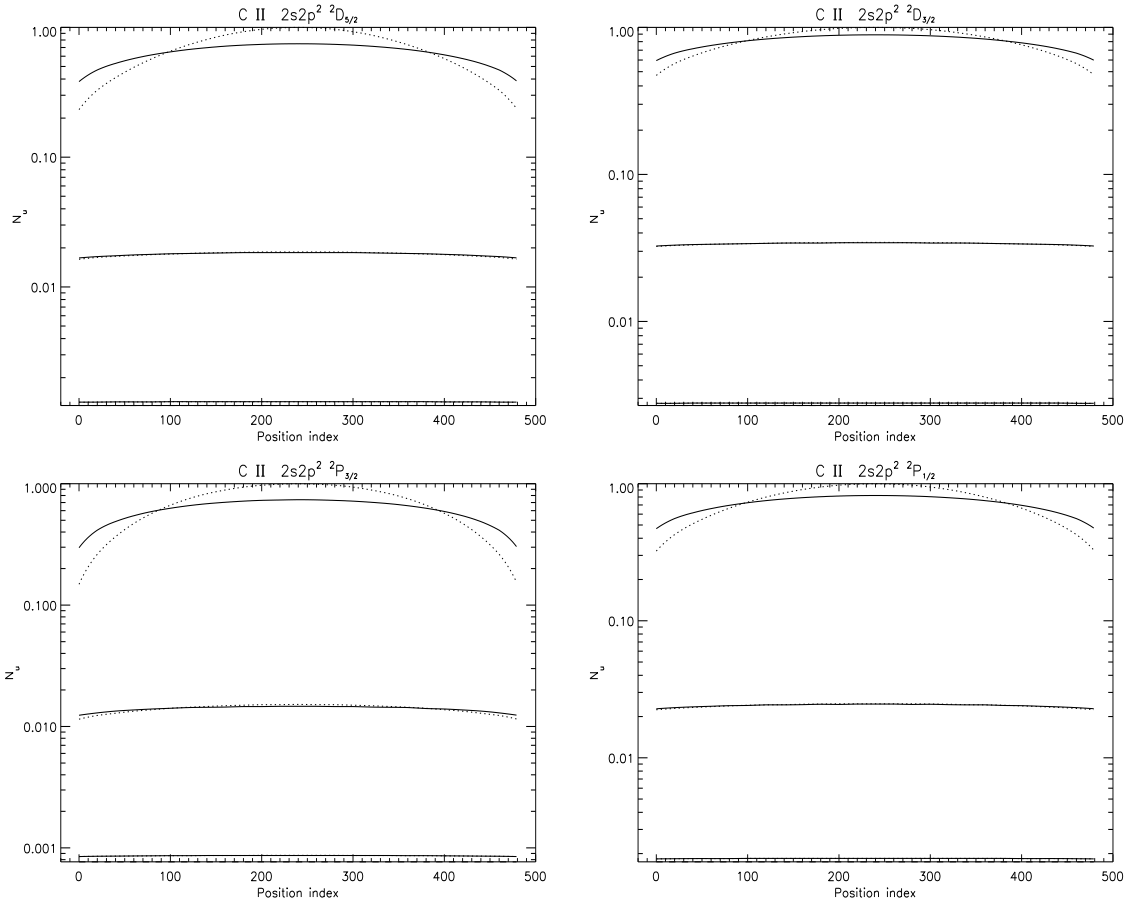

Figure 3.8: Upper level population densities versus spatial position for selected levels of C II. The solid lines correspond to calculations based on $\Lambda(\tau_0, x)$ for the same three sets of optical depths as in figs 3.5 and 3.6. The dotted lines represent the $\mathcal{G}(\tau_0, x)$ based calculations. Values are not absolute but are scaled so that the maximum population density value is unity.

From the above it is clear that the assumption that the source function is constant in space does not lead to an accurate calculation of the absorption factor, particularly

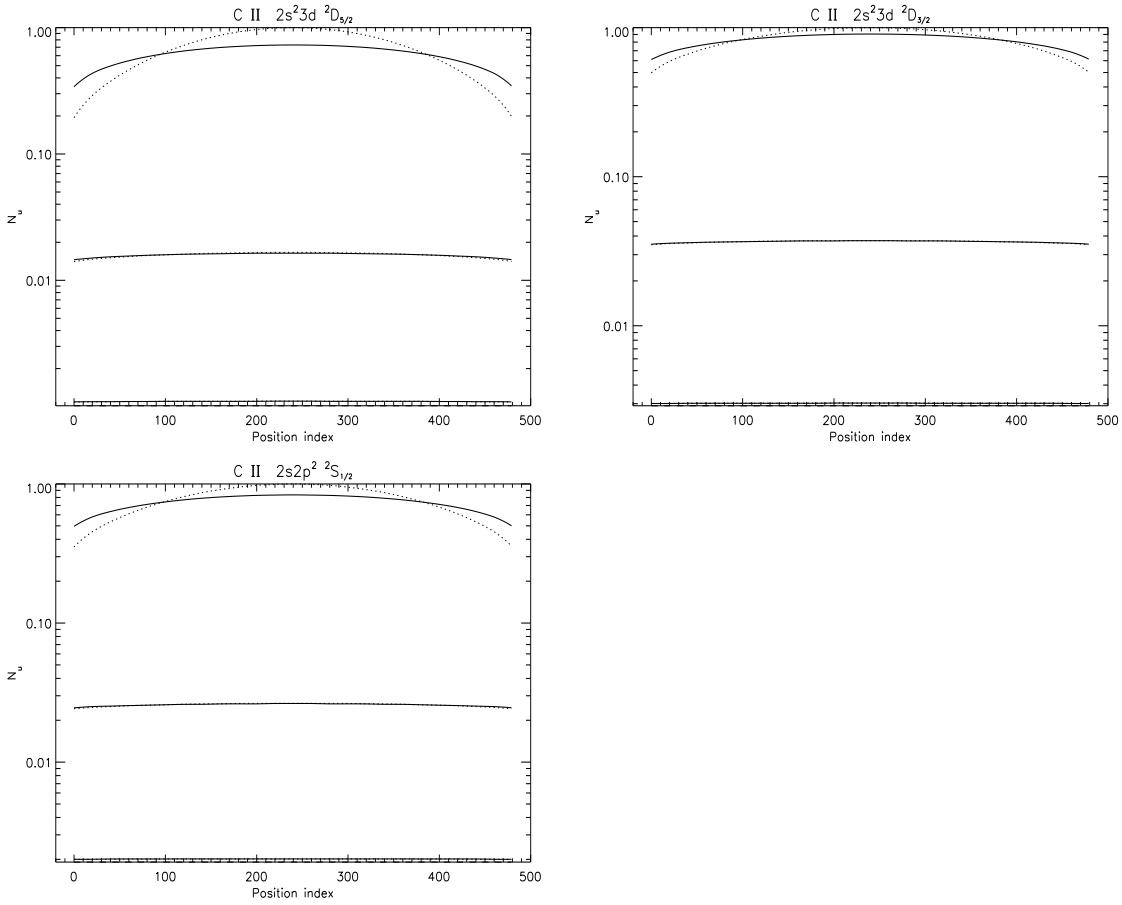

Figure 3.9: Upper level population densities versus spatial position for selected lines of C II. The solid and dotted lines are as in fig. 3.8. Values are not absolute but are scaled so that the maximum population density value is unity.

at the edge of the emitting layer. More important, however, is the validity of $\mathcal{G}(\tau_0, x)$ in predicting the population distributions. Figs 3.8 and 3.9 show the upper level population distributions for C II for the three optical depths regimes considered in figs 3.5 and 3.6. In these figures the logarithmic scale hides somewhat the extent of the difference in the populations calculated using $\Lambda(\tau_0, x)$ as compared with those using $\mathcal{G}(\tau_0, x)$. Figs 3.10 and 3.11 shows this difference on a linear scale for the most optically thick case. It is evident that in these figures there is a difference in the two and that $\mathcal{G}(\tau_0, x)$ is largely ineffective. However, the effect of using $\Lambda(\tau_0, x)$, and thus including the variation of the source function due to opacity, is to decrease the

degree of distortion of the upper level. The *absolute* value of the average population modification is not distinctly different between the two calculations but the variation in space is visibly less in the $\Lambda(\tau_0, x)$ case.

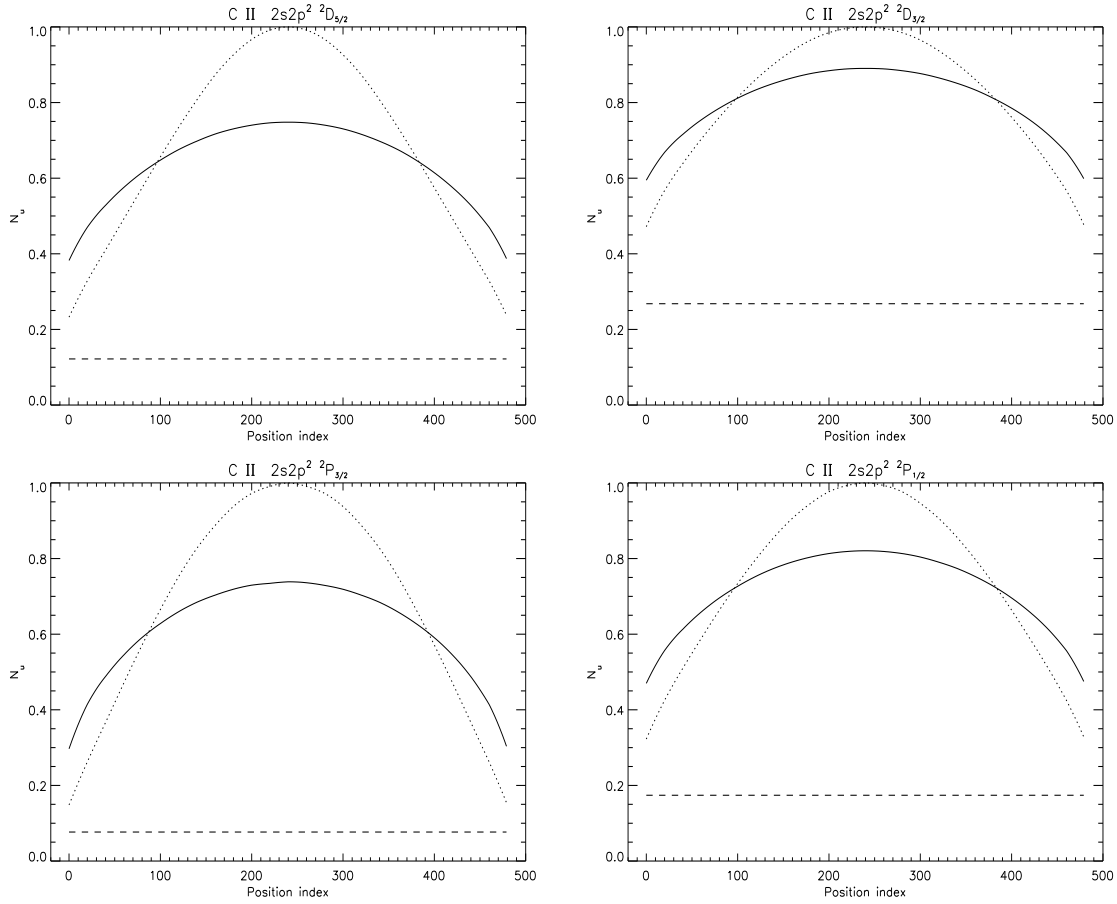

Figure 3.10: Upper level population densities versus spatial position for selected lines of C II as in figs 3.8 and 3.9 but just in the most optically thick case. The linear-linear scale reveals the degree of distortion of the upper level population density distribution for an optical depth of 10 in the control line (the C II $2s^2 2p^2 P_{3/2} - 2s2p^2\,^2P_{3/2}$ line at 904.143 Å). The solid and dotted lines are as in figs 3.8 and 3.9.

The subtle, indirect effects that influence lines such as the $2s^2 2p^2 P_{1/2} - 2s2p^2\,^2P_{3/2}$ line at 903.620 Å, evident in the absorption factors shown in figs 3.5 and 3.6, do not appear in the population distributions. This is because these indirect effects influence lines that share an upper level with lines that are thicker than themselves. These thicker partners, by virtue of their opacity, have $\Lambda(\tau_0, x)$ distributions that follow

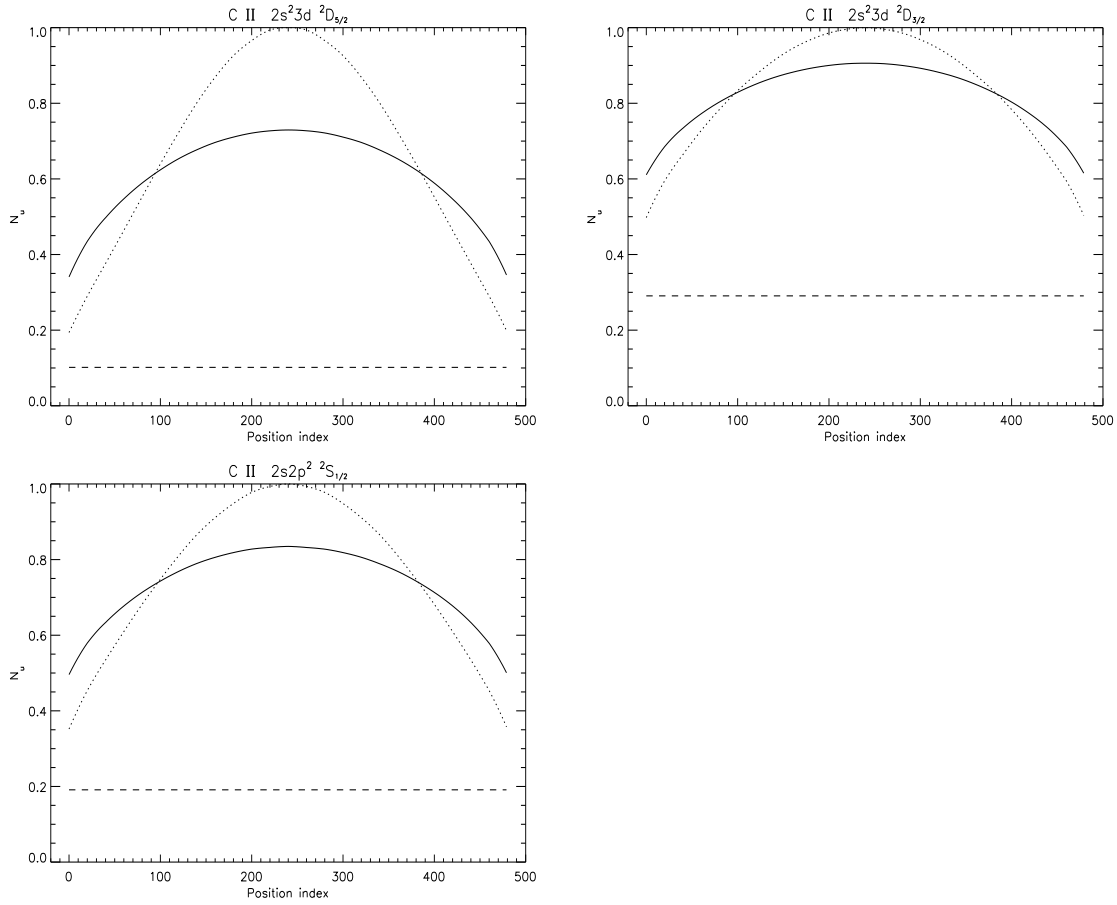

Figure 3.11: Upper level population densities versus spatial position for selected lines of C II as in fig. 3.10.

more closely the $\mathcal{G}(\tau_0, x)$ based distribution. These thicker lines, by virtue of their larger oscillator strengths (see eq. 2.14), have a more dominant role in the population calculation and so the indirect effects upon the absorption factors are minimised.

3.8 The exponential density case

The discussion so far has been restricted to the constant density case. Figures are shown in appendix A for the exponential density case. For this model the same conclusions follow.

3.9 Modelling emergent intensities

With opacity modified upper level population distributions calculated, emergent intensities may be obtained using eq. 3.18. Figs 3.12a and b show limb-brightening curves for the C II $2s^2 2p\,^2P_{3/2} - 2s2p^2\,^2P_{3/2}$ line at 904.143 Å calculated using eqs 3.18 and 3.25. For both atmosphere models considered in these figures it is clear that even with a disk centre optical depth of 10 the modified population makes little difference. Figs 3.13a and b show the same but for the C II $2s^2 2p\,^2P_{1/2} - 2s2p^2\,^2P_{3/2}$ line at 903.620 Å. This line shares its upper level with the 904.143 Å line and is considerably thinner than the latter. Thus its upper level is modified to a greater extent than its own optical depth would imply. It would be expected that for this line the population modification to the intensities would be more severe. However, as with the 904.143 Å line, there is only modest difference even in the most optically thick case. Indeed the difference is less than that for the 904.143 Å line.

Given the degree of distortion of the upper level population distribution evident in figs 3.10 and 3.11, the similarity between the $g\{\tau_0(x)\}$ based and $\bar{g}\{\tau_0\}$ based calculations is surprising. This is especially so given that the curves in figs 3.12 and 3.13 are scaled to match at disk centre. It is in moving away from disk centre toward the limb that the two results would be expected to deviate from one another the most since it is here that the geometric extension of the line-of-sight is minimal. In the vicinity of the limb the line-of-sight is extended, hence the total population modification is stretched and thus minimised with respect to the total line-of-sight optical depth.

To gain insight into this it is useful to generalise $\bar{g}\{\tau_0\}$ so that it may be expressed in the case where the source function is not constant.

3.9.1 The modified $\bar{g}\{\tau_0\}$

Following Behringer (1997) the line-of-sight averaged escape probability may be more generally defined as

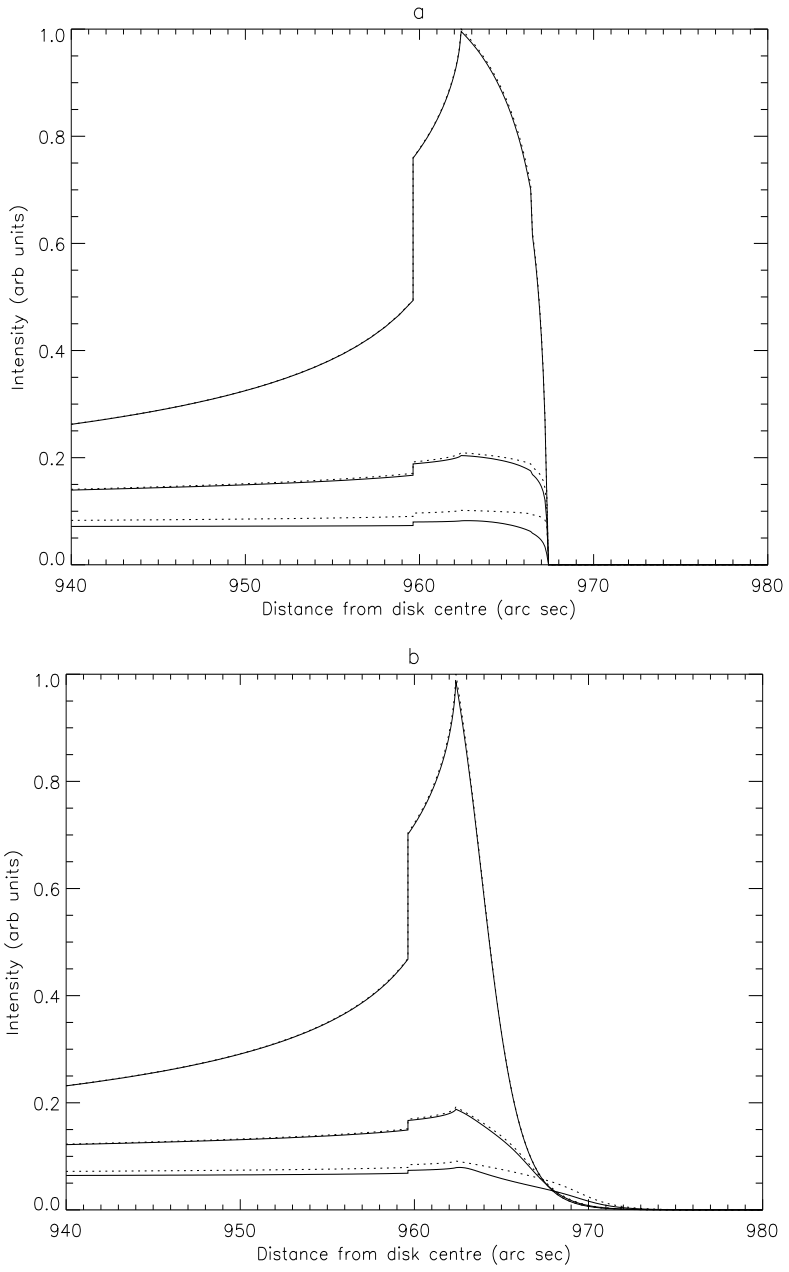

Figure 3.12: Predicted limb-brightening curves for the C II $2s^2 2p\,^2P_{3/2} - 2s2p^2\,^2P_{3/2}$ line at 904.143 Å calculated using $g\{\tau_0(x)\}$ with an opacity modified upper level population density distribution (solid lines) and using $\bar{g}\{\tau_0\}$ assuming constant source function (dotted lines) via eqs 3.18 and 3.25 respectively. Intensities are calculated in (a) a constant density model and (b) a model with density that decreases exponentially with height. Each contain three sets of curves corresponding to disk centre optical depths of 0.1, 1 and 10. The curves are scaled to match at disk centre.

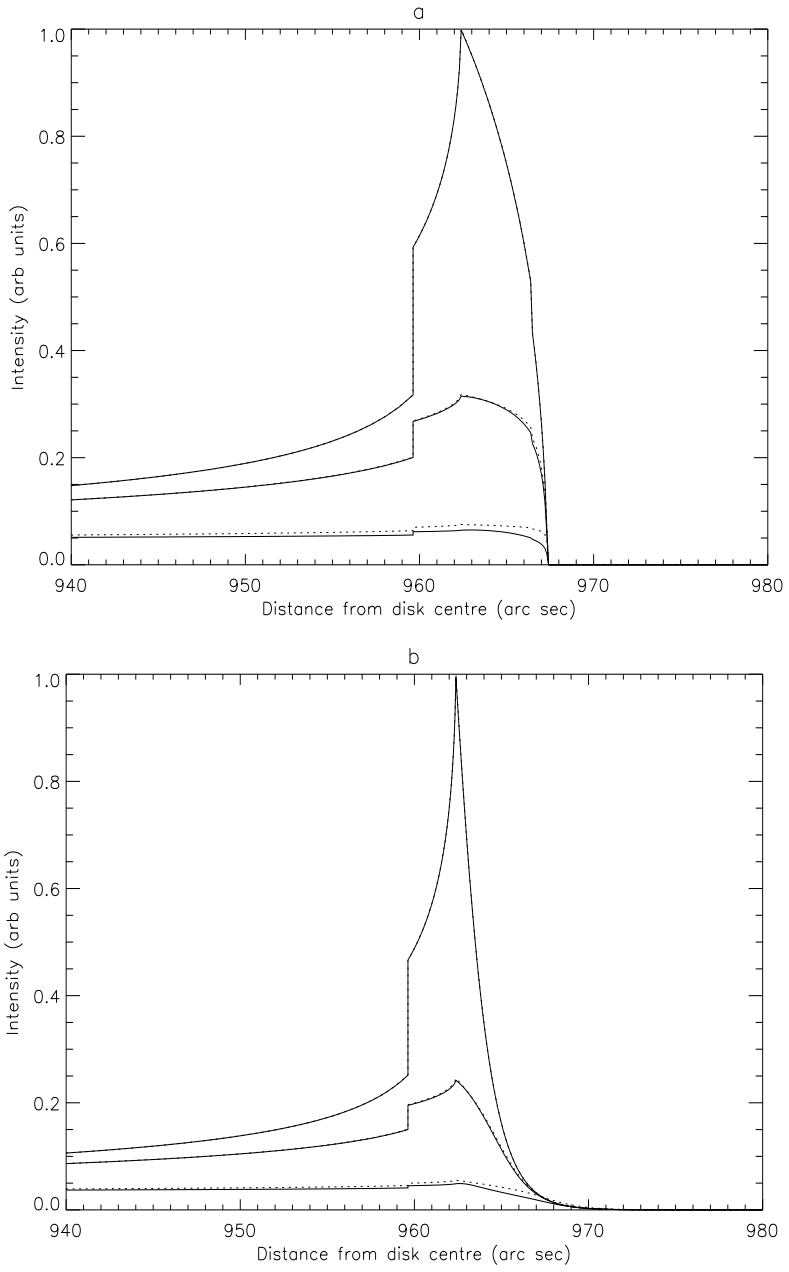

Figure 3.13: Predicted limb-brightening curves for the C II $2s^2 2p\,^2P_{1/2} - 2s2p^2\,^2P_{3/2}$ line at 903.620 Å calculated using $g\{\tau_0(x)\}$ with an opacity modified upper level population density distribution (solid lines) and using $\bar{g}\{\tau_0\}$ assuming constant source function (dotted lines) via eqs 3.18 and 3.25 respectively. (a) a constant density model and (b) a model with density that decreases exponentially with height. Each contain three sets of curves corresponding to disk centre optical depths of 0.02, 0.2 and 2. The curves are scaled to match at disk centre.

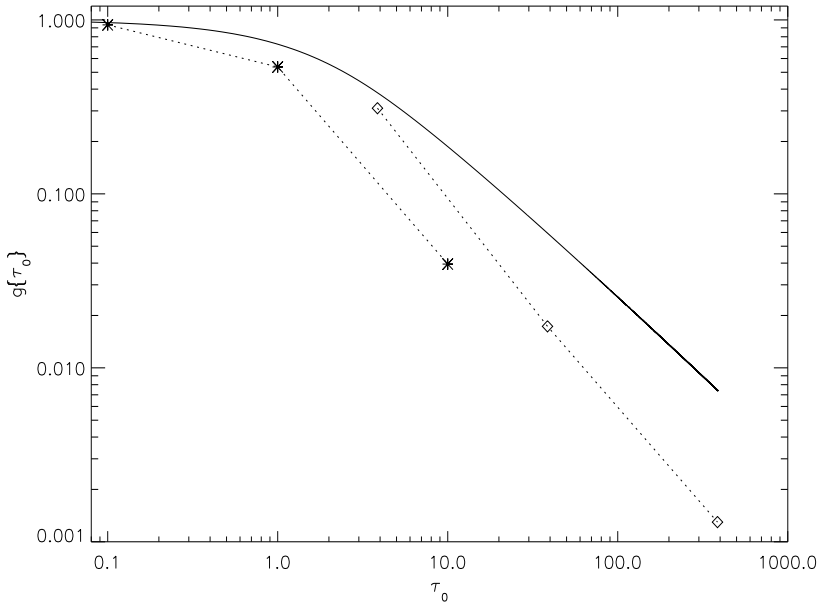

Figure 3.14: $\bar{g}\{\tau_0\}$ and $\bar{g}_r\{\tau_0\}$ versus τ_0 at disk centre and the limb shown on a log-log scale. The solid line shows $\bar{g}\{\tau_0\}$. The *'s correspond to $\bar{g}_r\{\tau_0\}$ at disk centre and the $\diamond$'s correspond to $\bar{g}_r\{\tau_0\}$ at the limb. The limb values are closer than the disk centre ones to the $\bar{g}\{\tau_0\}$ values. This is because the distortion of the upper level population density along the line-of-sight is less severe at the limb than at disk centre since the line-of-sight itself is geometrically extended.

$$\begin{aligned} \bar{g}_r[N_u(s), N_l(s), \tau_\nu] &\equiv \frac{I^{o.thick}}{I^{o.thin}} \\ &= \frac{\int_\nu \int_{l.o.s} N_u(s)\phi(\nu) exp\{-\tau_\nu\} ds d\nu}{\int_\nu \int_{l.o.s} N_u(s)\phi(\nu) ds d\nu} \end{aligned} \tag{3.35}$$

In general $\bar{g}_r[N_u(s), N_l(s), \tau_\nu]$ has a functional dependence upon the spatially resolved upper and lower level population densities, $N_u(s)$ and $N_l(s)$ but for particular choices of these, $\bar{g}_r[N_u(s), N_l(s), \tau_\nu]$ may be characterised purely as a function of optical depth, τ_0. Consequently $\bar{g}_r[N_u(s), N_l(s), \tau_\nu]$ may be written as $\bar{g}_r\{\tau_0\}$.

Since the optically thick emission must first be calculated for $\bar{g}_r\{\tau_0\}$ to be known, it is not a useful quantity for calculating optically thick emission. However, the comparison between $\bar{g}\{\tau_0\}$ and $\bar{g}_r\{\tau_0\}$ is insightful and is shown in fig. 3.14. The two are compared at disk centre and at the limb. As discussed above the difference

between $\bar{g}\{\tau_0\}$ and $\bar{g}_r\{\tau_0\}$ is less at the limb than at disk centre. This is because at the limb the population modification along the line-of-sight is minimised with respect to its optical depth due to the geometric extension of the line-of-sight in comparison with that at disk centre. For example, a disk centre optical depth of 1 translates, in the constant density model, to a limb optical depth of ~ 40. Yet the population modification along the line-of-sight at both disk centre and the limb is characterised by the smaller optical depth of 1.

There is an apparent discrepancy between figs 3.12 and 3.13 and fig. 3.14 as there is a more marked difference between $\bar{g}\{\tau_0\}$ and $\bar{g}_r\{\tau_0\}$ than there is between the intensity calculations based on $\bar{g}\{\tau_0\}$ and $g\{\tau_0(s)\}$. That is, it appears from figs 3.12 and 3.13 that the emergent fluxes are insensitive to the distortion of the source function due to opacity, yet fig. 3.14 indicates that the escape probability is sensitive.

The answer to this lies in the denominator of eq. 3.35, namely $I^{o.thin}$. This quantity, given by

$$I^{o.thin} = \int_{\nu} \int_{l.o.s} N_u(l)\phi(\nu) dl d\nu \tag{3.36}$$

is greater in the case in the case where the population modification is included because the population modification is an enhancement. The optically thick intensity is given by

$$I^{o.thick} = I^{o.thin} \times \frac{I^{o.thick}}{I^{o.thin}} = I^{o.thin}\bar{g}_r\{\tau_0\} \tag{3.37}$$

If the optically thin emission in the population modified case is labelled $I_r^{o.thin}$ and in the unmodified case it is labelled $I_u^{o.thin}$, and similarly for the optically thick emission, then

$$I_r^{o.thin} > I_u^{o.thin} \text{ and } \bar{g}_r\{\tau_0\} < \bar{g}\{\tau_0\} \Rightarrow I_r^{o.thick} \approx I_u^{o.thick} \tag{3.38}$$

which is true for optical depths even up to ~ 10.

3.9.2 The perspective of scattering into the line-of-sight

The effect of the enhancement of the upper level – or, in other words, the modification to the source function – due to opacity may be viewed from the perspective of

scattering *into* as well as out of the line-of-sight. In radiative transfer theory the term *scattering* has a very specific meaning. Specifically, a scattering event is one in which a photon is absorbed and re-emitted before the absorbing atom or ion suffers any collisions leading to excitation, de-excitation or ionisation. If collisions do occur after the photon is captured and before another photon is emitted then the captured photon is said to be *absorbed*. The distinction between these two events is significant when considering frequency redistribution since scattering leads to a relationship between the emission and absorption profiles. This was discussed in sec. 1.3.1. Within escape probability theory such subtleties are not considered since the techniques are invalid within the optical depth regime where partial frequency redistribution becomes an important issue (see chapter 6). In the context of escape probability theory, scattering into the line-of-sight refers to any absorption of a photon that leads to emission in a line somewhere along a line-of-sight in the direction of that line-of-sight.

Kastner & Bhatia (1992), following the work of Jordan (1967), wrote that the fraction of photons created, escaping in line i is

$$b_i p_{e,j} = \frac{b_i \ \vec{p}_{f,j}}{1 - \sum_i b_i (1 - p_{d,i})(1 - \bar{p}_{f,i})(1 - \vec{p}_{f,i})} \tag{3.39}$$

where $p_{d,i}$ is the photon loss probability (Kastner, 1981), $\vec{p}_{f,j} = p_f(\hat{\nu}, \vec{k}, \tau : 1) \equiv \bar{g}\{\tau_0\}$, and $\bar{p}_{f,i} = p_f(\hat{\nu}, \vec{k}, \tau : 0)$. $\bar{p}_{f,i}$ is the mean probability that a photon emitted anywhere in the layer will travel to the surface and escape. This was described in chapter 2. This approach assumes that the emission at a point is characterised by an optically thin (unmodified) population structure but includes contributions at each point due to light scattered into the line-of-sight from all other points. Thus

$$I^{(o.thick)} \sim \int_{l.o.s.} N_u^{(o.thin)}(s) A_{u\to l}^{(o.thick)} g\{\tau_0(s)\} ds \tag{3.40}$$

where $A_{u\to l}^{(o.thick)}$ is $A_{u\to l}$ divided by the denominator of eq. 3.39.

In the work presented in sec. 3.9 eq. 3.40 is written differently. Specifically, if at each point along a line-of-sight an optically thick population structure is obtained via the solution of eq. 2.6, then the intensity is

$$I \sim \int_{l.o.s.} N_u^{(o.thick)}(s) A_{u\to l}^{(o.thin)} g\{\tau_0(s)\} ds \tag{3.41}$$

In this picture emission at a point is characterised by an optically thick population structure and the only effect of opacity thereafter (excluding, that is, partial frequency redistribution) is due to scattering out of the line-of-sight. There is no scattering into the line-of-sight in this picture as the enhancement due to photons absorbed and re-emitted in line i is taken into account in the $\bar{I}_\nu$ term in eq. 2.6.

Bhatia & Kastner (1999) calculated optically thick populations iteratively starting from an optically thin solution and assuming that the source function is constant throughout the emitting layer. Here a similar approach is taken but for each iteration the populations are calculated at every point throughout the layer using the resolved absorption factor – the absorption factor as a function of space – to obtain an optically thick upper level population distribution. Thus in this work the spatial variation of the source function is included within the iterative process.

3.10 The implications of a spatially varying source function upon escape probability techniques

It has been shown above that the modification to the source function due to photo-absorption has a minimal effect upon the validity of $\bar{g}\{\tau_0\}$ (via eq. 3.25) in describing optically thick spectral emission for disk centre optical depths up to (and perhaps beyond) ~ 10. The viewpoint of scattering into the line-of-sight has been introduced to separate out the spatial variation of the source function, $S_\nu(\mathbf{x})$, due to opacity from that due to the more general variation due to the changes in (T_e, N_e) throughout the region of line formation. It was shown in sec. 3.1 that this variation is likely to be severe in the C II and C III emitting layers. The assumption that a single (T_e, N_e) pair is sufficient to describe the C II and C III emitting layers has thus far not been justified and will be addressed later in chapter 6. However, consider for the moment the intensity from a layer of variable source function. Such emission is given by

$$I \sim \int_0^L S(s) g(\kappa_0 \int_0^s N_l(s')ds')ds \tag{3.42}$$

Here it is assumed that the source function, $S(s)$, is independent of frequency. Putting

$$\begin{aligned} t(s) &= \kappa_0 \int_0^s N_l(s')ds' \\ \Rightarrow \frac{dt}{ds} &= \kappa_0 N_l(s) \end{aligned} \tag{3.43}$$

leads to

$$\begin{aligned} I &\sim \int_0^L S(s(t))g(t)dt \\ \Rightarrow I &\sim \bar{N}_l \bar{g}\{\tau_0\} L f_{los}\{\tau_0\} \end{aligned} \tag{3.44}$$

where

$$f_{los}\{\tau_0\} = \int_0^L \frac{\tilde{N}_u(t)}{\tilde{N}_l(t)} \frac{g(t)}{\bar{g}\{\tau_0\}} dt \tag{3.45}$$

$f_{los}\{\tau_0\}$ is in general line-of-sight and optical depth dependent. The validity of modelling branching ratios and limb-brightening curves using eq. 3.25 hinges upon the nature of the dependence of $f_{los}\{\tau_0\}$ on τ_0 and line-of-sight.

Eq. 3.44 may be written as

$$I \sim \tilde{N}_l \bar{g}\{\tau_0\} L \tag{3.46}$$

where $\tilde{N}_l = \bar{N}_l f_{los}\{\tau_0\}$ is some representative upper level population density and is a function of optical depth and line of sight. The optical depth diagnostic described in sec. 2.1.1 depends upon the cancellation of the density terms in eq. 3.25. The fact that two lines in an intensity ratio arise from a common upper level is no longer guarantee that this cancellation occurs. However, since the diagnostic applies to one line-of-sight at a time, the dependence of $f_{los}\{\tau_0\}$ on line-of-sight is irrelevant.

For the time being it is assumed that $f_{los}\{\tau_0\} = const.$ This will be justified in chapter 6.

3.11 Concluding remarks

The spatially resolved absorption factor, $\Lambda(\tau_0, x)$, that has been develop here for a plane parallel stratified atmosphere, provides a route to examining the implications of

the assumption of constant source function on the validity of the escape probability technique. In particular, it enables the effect of scattering into the line-of-sight to be examined in a consistent manner. It is found that the $\mathcal{G}(\tau_0, x)$ quantity is generally ineffective for describing the spatial variation of absorption characteristics in spectral lines. This deficiency is due to coupling of lines that share a common upper level. Absorption of photons in an optically thick line will lead to a distortion of the upper level population distribution of that line. This will in turn influence the emission and thus also the absorption in that same line and also in other lines stemming from that same upper level. This coupling influences most markedly lines that share an upper level with a line that is more optically thick.

This deficiency in the $\mathcal{G}(\tau_0, x)$ quantity is minimised at layer centre. At an optical depth of 10 in the control line (the C II $2s^2 2p\,^2P_{3/2} - 2s2p^2\,^2P_{3/2}$ line at 904.143 Å), $\mathcal{G}(\tau_0, D/2)$ and $\Lambda(\tau_0, D/2)$ differ by $\sim 30\%$. However, at an optical depth of 1 in the control line the difference is only a few percent and the two quantities both vary monotonically with optical depth (see fig. 3.7a). Thus $\bar{\bar{g}}\{\tau_0/2\}$ is appropriate for describing the modification to the population structure due to opacity for a range of optical depths. Furthermore only modest scaling of this quantity would extend its range of validity up to an optical depth of 10 or more. The value for optical depth at disk centre of the control line deduced in chapter 2 was 1.76. This was the largest of all the C II lines and thus the $\bar{\bar{g}}\{\tau_0/2\}$ is appropriate for the classification of the C II spectral lines. The maximum optical depth in the C III lines was 0.156 which is well within the regime where $\bar{\bar{g}}\{\tau_0/2\}$ is valid.

The modified population density distributions do not display such sensitivity to the coupling effects described above since they are controlled by the strongest, and thus thickest lines which are the least influenced by these indirect effects. Moreover the predicted limb brightening curves show less sensitivity. These curves indicate that for $\tau_0 \sim 10$ in the control line, scattering into the line-of-sight is non-negligible. At optical depths less than this the modification to the source function due to opacity is not manifested in the emergent intensities. This implies an upper limit to the line-of-sight averaged escape probability, $\bar{g}\{\tau_0\}$, of $\sim \tau_0 = 10$. This is identical to the upper limit found by Kastner (1999) based on an intensity/linewidth method to

deduce optical depths from spectral observations using escape probabilities.